# RH and $O_3$ concentration as two prerequisites for sulfate formation

Yanhua Fang[1#] and Chunxiang Ye[1#], Junxia Wang[1], Yusheng Wu[1], Min Hu[1], Weili Lin[2], Fanfan Xu[1], Tong Zhu[1*]

[1]BIC-ESAT and SKL-ESPC, College of Environmental Sciences and Engineering, Peking University, Beijing, 100871, China
[2]College of Life and Environmental Sciences, Minzu University of China, Beijing 100081, China

[#]These authors contributed equally to the paper.

[*]*Correspondence to*: Tong Zhu (tzhu@pku.edu.cn)

**Abstract.** Sulfate formation mechanisms have been discussed extensively but are still disputed. In this work, a year-long particulate matter ($PM_{2.5}$) sampling campaign was conducted together with measurements of gaseous pollutant concentrations and meteorological parameters in Beijing, China, from March 2012 to February 2013. The sulfur oxidation ratio (SOR), an indicator of secondary sulfate formation, displayed a clear summer peak and winter valley, even though no obvious seasonal variations in sulfate mass concentration were observed. A rapid rise in the SOR was found at a RH threshold of ~45 % or an $O_3$ concentration threshold of ~35 ppb, allowing us to first introduce the idea that RH and $O_3$ concentrations are two prerequisites for rapid sulfate formation via multiphase reactions. In the case of the RH threshold, this is consistent with current understanding of the multiphase formation of sulfate, since it relates to the semisolid-to-liquid phase transition of atmospheric aerosols. Correlation analysis between SOR and AWC further backed this up. In the case of the $O_3$ concentration threshold, this is consistent with the consumption of liquid oxidants in multiphase sulfate formation. The thresholds introduced here lead us to better understanding of the sulfate formation mechanism and sulfate formation variations. $H_2O_2$ might be the major oxidant of sulfate formation, since another liquid phase oxidant, $O_3$, has previously been shown to be unimportant. The seasonal variations in sulfate formation could be accounted for by variations in the RH and $O_3$ prerequisites. For example, over the year-long study, the fastest $SO_2$-to-sulfate conversion occurred in summer, which was associated with the highest values of $O_3$ (and also $H_2O_2$) concentration and RH. The SOR also displayed variations with pollution levels, i.e., the SOR increased with $PM_{2.5}$ in all seasons. Such variations were primarily associated with a transition from the slow gas phase formation of sulfate to rapid multiphase reactions, since RH increased higher than its prerequisite value of around 45% as pollution evolved. In addition, the self-catalytic nature of sulfate formation (i.e., the formation of hydrophilic sulfate aerosols under high RH conditions results in an increase in aerosol water content, which results in greater particle volume for further multiphase sulfate formation) also contributed to variations among the pollution scenarios.

## 1 Introduction

Beijing, the capital of China, suffers from serious air pollution due to its rapid economic growth and urbanisation (Hu et al., 2015). The chemical composition and sources of fine particulate matter ($PM_{2.5}$) in Beijing have been studied extensively (Han et al., 2015; Lv et al., 2016; Zhang et al., 2013; Zheng et al., 2005). Secondary components, especially sulfate, nitrate, and ammonium (SNA), are the main contributors to $PM_{2.5}$ (Huang et al., 2014a). On the most severely polluted days, SNA account for more than half of total $PM_{2.5}$ mass concentrations and play a more important role than on clean days (Quan et al., 2014; Wang et al., 2014b; Zheng et al., 2015b).

The kinetics and mechanisms of the formation of sulfate, a major component of SNA, are complex and remain unclear (Ervens, 2015; Harris et al., 2013; Warneck, 2018). For example, two key questions concerning sulfate formation are: (1) exactly how do various parameters (oxidants, catalysts, meteorological conditions, etc.) influence sulfate formation, and (2) how do multiple formation routes compete and contribute together to sulfate formation under ambient conditions. In general, sulfate is produced from $SO_2$ via gas phase oxidation reactions involving the hydroxide radical (OH) and Criegee intermediates (Gleason et al., 1987; Sarwar et al., 2014; Vereecken et al., 2012), heterogeneous reactions (mainly on dust aerosols), and multiphase transformations with $O_3$, $H_2O_2$, or $O_2$ (catalysed by transition metal ions (TMIs) (i.e., TMIs + $O_2$) and $NO_2$ ($NO_2$ + $O_2$)) as liquid phase oxidants, which occur mainly in clouds but also in aerosol droplets near the ground (Zhu et al., 2011).

Due to the major role of multiphase transformations, sulfate production is presumed to be self-catalysed, i.e., the formation of hydrophilic sulfate aerosols under high relative humidity (RH) conditions results in an increase in aerosol water content (AWC), which results in greater particle volume for further multiphase sulfate formation (Cheng et al., 2016; Pan et al., 2009; Xu et al., 2017). Analyses of the correlation of sulfate formation with RH and AWC have been conducted to test this hypothesis, using the concept of the sulfur oxidation ratio (SOR), defined as the molar ratio of sulfate to total sulfur (= sulfate + $SO_2$). It is used to indicate the magnitude of the secondary formation of sulfate and expressed as (Wang et al., 2005):

$$\mathrm{SOR} = \frac{n_{SO_4^{2-}}}{n_{SO_4^{2-}} + n_{SO_2}}, \qquad \text{(Eq. 1)}$$

where $n_{SO_4^{2-}}$ and $n_{SO_2}$ represent the molar concentrations of sulfate and $SO_2$, respectively. Even though regional transport or intrusion of $SO_2$ or sulfate (or local sulfate emissions) would modify the SOR, it has still often been a relatively good proxy of secondary sulfate formation (i.e., local $SO_2$-to-sulfate conversion). For example, Sun et al. (2014; 2013) found positive correlations between the SOR and RH, and observed rapid increases in SORs at elevated RH levels. Xu et al. (2017) found positive correlations of the SOR with both RH and AWC. Multiphase transformation routes, including $O_3$ oxidation, TMIs + $O_2$, and $NO_2$ + $O_2$, are pH-sensitive and suppressed at low pH (Seinfeld and Pandis, 2006). Sulfate production raises the acidity of aerosols and therefore the multiphase transformations of sulfate are presumed to be self-constrained (Cheng et al., 2016). For example, a significant contribution from the $O_3$ oxidation route can only be expected under alkaline conditions (e.g., sea-salt), otherwise, $O_3$ oxidation is a minor pathway for sulfate formation (Alexander et al., 2005; Sievering et al., 2004). How the self-constraining nature of sulfate formation influences the relative significance of the TMIs + $O_2$ and $NO_2$ + $O_2$ routes is

still under debate. Cheng et al. (2016) proposed that the $NO_2 + O_2$ route is important during severe haze events under neutral pH conditions (He et al., 2018; Wang et al., 2016). Guo et al. (2017) suggested that aerosols are acidic in Beijing (except for during the limited cases of dust or sea-salt events), casting doubt on the importance of the $NO_2 + O_2$ route in sulfate formation (Liu et al., 2017a). According to laboratory-based Raman spectroscopy studies, sulfate can be produced via the aqueous oxidation of $SO_2$ by $NO_2 + O_2$, with an $SO_2$ reactive uptake coefficient of $10^{-5}$, which represents an atmospherically relevant value (Yu et al., 2018), whereas others have suggested that this route is of minor importance in the atmosphere (Li et al., 2018; Zhao et al., 2018). In addition, Xie et al. (2015) proposed that $NO_2$ could enhance the formation of sulfate in certain cases, for example, in biomass burning plumes or dust storms (He et al., 2014). Evaluation of the contribution of TMIs + $O_2$ reactions appears to be more complex since it depends on aerosol acidity, solubility, oxidation state, and the synergistic effects of different TMIs (Deguillaume et al., 2005; Warneck, 2018).

The compensating effects among AWC, aerosol acidity, and the concentrations of precursors and catalysts show that the kinetics and mechanisms of sulfate formation are highly complex. It can be inferred that there is competition between the various routes, with dependences on atmospheric conditions (e.g., seasonal and pollution level variations) likely, but this has not received much research attention previously. Here, daily $PM_{2.5}$ samples were collected in Beijing from March 2012 to February 2013 and their chemical composition was analysed. The main parameters that influenced sulfate formation (i.e., RH, $O_3$ concentration, TMIs, etc.) were determined. This valuable dataset enabled us to explore: (1) the specific role of each influencing factor in sulfate formation, and (2) how multiple sulfate formation routes compete in different seasons and under various pollution scenarios.

## 2 Measurements and methodology

### 2.1 Measurements

#### 2.1.1 Measurement stations

The two measurement stations are shown in Fig. 1. The PKU station (116.30 °E, 39.99 °N) is about 20 m above ground level at the campus of Peking University, Beijing, China (Liang et al., 2017). Daily $PM_{2.5}$ samples were collected using a four-channel sampler (TH-16A; Wuhan Tianhong Instruments, China) at a flow rate of 16.7 L $min^{-1}$ from 1 March 2012 to 28 February 2013. The gaseous pollutants $SO_2$, $NO_x$, and $O_3$ were measured with a pulsed fluorescence $SO_2$ analyser (Model 43i TLE; Thermo Fisher Scientific, Waltham, MA, USA), chemiluminescence NO–$NO_2$–$NO_x$ analyser (Model 42i TL; Thermo Fisher Scientific), and an ultraviolet photometric $O_3$ analyser (Model 49i; Thermo Fisher Scientific), respectively. Temperature and RH were also monitored (MSO; Met One Instruments, Grants Pass, OR, USA). Solar radiation data were obtained from the Beijing Meteorological Observatory Station (116.47 °E, 39.81 °N). Daily averages were used for all analysis conducted in this work.

### 2.1.2 Filter sampling and analysis

Each $PM_{2.5}$ sample set consisted of one quartz filter (47 mm; Whatman QM/A, Maidstone, England) and three Teflon filters (47 mm; pore size = 2 μm; Whatman PTFE). The quartz filters were baked for 5.5 h at 550 ℃ before use. The Teflon filters were weighed in a weighing room before and after sampling using a delta range balance (0.01 mg/0.1 mg precision; AX105; Mettler Toledo, Switzerland). To minimise contamination, all Teflon filters were placed in a super clean room (temperature = 22 ±1 ℃; RH = 40 ±2 %) for 24 h before being weighed. After sampling, all filters were stored at −20 ℃ prior to analysis. Water soluble cations ($Na^+$, $NH_4^+$, $K^+$, $Mg^{2+}$, and $Ca^{2+}$) and anions ($SO_4^{2-}$, $NO_3^-$, $Cl^-$, and $F^-$) were measured using ion chromatography (ICS-2500 and ICS-2000; DIONEX, USA). Trace elements (Na, Mg, Al, Ca, Ti, Cr, Mn, Fe, Co, Ni, Cu, Zn, Se, Mo, Cd, Ba, Tl, Pb, Th, and U) were analysed by inductively coupled plasma–mass spectrometry (ICP–MS, X-Series; Thermo Fisher Scientific). Organic carbon (OC) and elemental carbon (EC) were measured using a thermal/optical carbon analyser (RT-4; Sunset Laboratory Inc., Tigard, OR, USA). The procedure for the measurement of water soluble Fe has been described in detail in a previous study (Xu et al., 2018).

### 2.2 Estimation of the mass concentrations of $PM_{2.5}$ components

The chemical components of $PM_{2.5}$ were divided into eight categories: sulfate, nitrate, ammonium, organic matter (OM), EC, minerals, trace element oxides (TEOs), and others. The mass concentrations of OM, minerals, and TEOs were calculated from OC, Al, and trace element concentrations, respectively. The details of this method are provided in the supplementary information (SI). For minerals, validation of the method using only Al to represent all minerals is shown in Fig. S1. TEOs mostly originated from anthropogenic sources (Fig. S2).

### 2.3 Quality assurance and quality control

The $PM_{2.5}$ sampling instruments were cleaned and calibrated every 2–3 months. Before the daily filter replacement, filter plates were scrubbed with degreasing cotton that had been immersed in dichloromethane. For water soluble ions, OC/EC, and trace element measurements, standard solutions were analysed before each series of measurements. The $R^2$ values of the calibration curves were all > 0.999. For water soluble ion measurements, beakers, tweezers, and vials were cleaned with deionised water (18.2 MΩ; Milli-Q, USA) three times before use. Certified reference standards (National Institute of Metrology, China) were used for calibration. For OC/EC measurements, tweezers and scissors were scrubbed with degreasing cotton immersed in dichloromethane for every filter. Total organic carbon (TOC) was calculated based on calibration with external standard solutions. For trace element measurements, containers and tweezers were cleaned three times with nitric acid before use, and the analysis of a certified reference standard (NIST SRM-2783) was used to verify accuracy. The recovery of all measured trace elements fell within ± 20 % of their certified values. For gaseous pollutants and meteorological parameters, all instruments were maintained and calibrated weekly based on manufacturers' protocols.

## 3 Results and discussion

### 3.1 General description

The annual and seasonal mean (±one standard deviation (SD)) concentrations of $PM_{2.5}$ and its seven major known components are summarised in Table 1. The annual mean $PM_{2.5}$ concentration was 84.1 (± 63.1) μg $m^{-3}$, which is more than two times greater than the Chinese National Ambient Air Standard annual mean concentration of 35 μg $m^{-3}$. On 145 of the 318 (46 %) measurement days, daily mean $PM_{2.5}$ concentrations were above the Chinese National Ambient Air Standard 24 h mean concentration of 75 μg $m^{-3}$. Time series of $PM_{2.5}$ concentrations and its seven major known components are shown in Fig. 2. Seasonal variations in $PM_{2.5}$ loading are obvious, with spring and winter peaks and summer and autumn valleys. OM and EC concentrations displayed common seasonal variations, with a plateau from mid-October to mid-February and a valley in summer (Fig. 2), which resembles the variations in $PM_{2.5}$, $K^+$, $Cl^-$, and $F^-$ (Figs. 2 and 3). The seasonal variations in minerals also indicate an important contribution of dust events to $PM_{2.5}$ loading during spring, which is a well-known phenomenon (Zhang et al., 2003; Zhuang et al., 2001). TEOs displayed no obvious seasonal variations (Fig. 2). SNA accounted for more than one-third of $PM_{2.5}$ annually and showed similar seasonal variations to that of $PM_{2.5}$ (Fig. 2), with the notable exception that sulfate became the highest contributor to $PM_{2.5}$ (~25 %) in summer (Fig. 4). The summer peak in sulfate could be accounted for by fast secondary formation, as will be discussed later.

On an annual basis, the seven major known components accounted for over 80 % of $PM_{2.5}$ (Fig. 4). The diversity of the seasonal variations in $PM_{2.5}$ and its major components found in our study imply that there were seasonal variations in both the primary sources and secondary formation of $PM_{2.5}$.

### 3.2 Influence of various parameters on sulfate formation

To further explore the parameters that influenced sulfate formation, SORs were plotted against RH and the concentrations of $O_3$, $NO_2$, and Fe (total Fe, including both water soluble and water insoluble Fe), which is a major tracer of transition metals (Figs. 5 and 6).

As shown in Fig. 5a, an RH threshold of ~45 % was critical for efficient $SO_2$ oxidation (i.e., a high SOR). Such a threshold effect was thought to be reasonable given that AWC increases sharply when RH was above a threshold of 45 %, at which the aerosol undergoes a phase transition from a (semi-)solid particle to a droplet (Pan et al., 2009; Russell and Ming, 2002). Further correlation analysis between SOR and AWC further supports that the multiphase reactions are responsible for sulfate formation. (Fig. S3). Our observation of a daily average RH threshold of ~45 % is in line with previous reports of 40–50 % (Liu et al., 2015; Quan et al., 2015; Xu et al., 2017; Yang et al., 2015; Zheng et al., 2015b), but is slightly lower than the *in situ* phase transition threshold RH of 50–60 % previously observed in Beijing (Liu et al., 2017b). Correlation analysis of SOR and RH (or AWC) has often been conducted in previous studies. For example, Wang et al. (2005) found a weak positive correlation of SORs with RH ($R$ = 0.38), while Sun et al. (2006) found a strong positive correlation ($R$ = 0.96). However, the analysis in the present work and those of a few previous studies revealed that the relationship between the SOR and RH is

nonlinear (Sun et al., 2013; Sun et al., 2014; Zheng et al., 2015b). In fact, the RH threshold suggests that high RH (or AWC) is a prerequisite for fast sulfate formation via multiphase reactions, which are known to account for the majority of sulfate accumulation.

From the large scattering of data points around the fit line in Fig. 5a, it might be inferred that RH was not the only prerequisite for fast $SO_2$-to-sulfate conversion. As shown in Fig. 5b, a significant increase in the SOR was also observed at an $O_3$ concentration threshold of ~35 ppb. High $O_3$ concentrations (i.e., > 35 ppb) were accompanied by high SOR values of ~0.4 (right-hand side of Fig. 5b). Correlation analyses of SORs with $O_3$ have been conducted but inconsistent results were reported. Wang et al. (2005) found a weak positive correlation between SORs and $O_3$ ($R$ = 0.47) for continuous observations in Beijing during 2001–2003. However, Liu et al (2015) found a weak negative correlation between SORs and $O_3$ ($R$ = −0.53, $p$ = 0.01) during a haze episode in September 2011. Zhang et al. (2018) found no correlation between SORs and $O_3$ during winter haze days in 2015. Quan et al. (2015) found that the SOR decreased with $O_3$ when $O_3$ concentrations were lower than 15 ppb, but increased with $O_3$ when $O_3$ concentrations were higher than 15 ppb, for observations made during autumn and winter 2012. In the present study, our observations revealed that the relationship between the SOR and $O_3$ concentration, like RH, was nonlinear and that a high $O_3$ concentration was another prerequisite for fast sulfate formation. Such a conclusion was a surprise first, since $O_3$ oxidation was not thought to be a major route for $SO_2$-to-sulfate conversion (He et al., 2018; Sievering et al., 2004). However, as a primary precursor to OH radicals and $H_2O_2$ (via $HO_2$), (Lelieveld et al., 2016; Lu et al., 2017), high $O_3$ concentrations (e.g., > 35 ppb) correspond to a high concentration of oxidants, which favors multiphase sulfate formation and thus a high SOR, whereas low $O_3$ concentrations suggest a lack of available oxidants for multiphase $SO_2$-to-sulfate conversion and thus a low SOR. In addition, the simultaneous occurrence of low SORs and low $O_3$ concentrations had a secondary cause. Low $O_3$ concentrations in the Beijing urban area were often due to the titration of $O_3$ by NO (Li et al., 2016), which accumulated together with $SO_2$ (Fig. S4). The accumulation of $SO_2$, which "diluted" the SOR (Eq. 1), was thus naturally accompanied by the titration of $O_3$. The L-shaped dependence of the SOR on several other primary pollutants, such as EC, NO, and Se (Fig. S5), further confirmed this secondary cause. Therefore, the accumulation of primary pollutants might also help to explain the low SOR values of ~0.1 on the left-hand side of Fig. 5b, in addition to the lack of available oxidants for multiphase $SO_2$-to-sulfate conversion.

The large scattering of data points around the fit line in Fig. 5b suggests that $O_3$ concentration, like RH, was not the only prerequisite for fast $SO_2$-to-sulfate conversion. The dependence of the SOR on RH was separated into low (< 35 ppb) and high (> 35 ppb) $O_3$ groups (solid black circles and solid blue circles, respectively, in Fig. 5a). SOR values above the fit line are found mostly for the high $O_3$ group. After the dependence of the SOR on $O_3$ concentration was separated into low (< 45 %) and high (> 45 %) RH groups (solid black circles and solid blue circles, respectively, in Fig. 5b), a similar pattern was found for the high RH group. In other words, fast multiphase $SO_2$-to-sulfate conversion could only occur when both $O_3$ and RH exceeded their respective thresholds simultaneously.

The seasonal variation of such thresholds of RH and $O_3$ were further discussed. As show in Fig. 6, RH threshold was roughly around 45 % during all four seasons in Beijing. While the threshold of $O_3$ varied among seasons (Fig.7). A turning

point of 25–40 ppb was observed for fast SOR increase in spring, summer and autumn, while the turning point is not clear due to lack of high $O_3$ data in winter. The variation of $O_3$ threshold value might be due to the shift of $O_3$-$H_2O_2$ relationship which might be modified by temperature etc. in different seasons. Despite of the variation of thresholds of RH and $O_3$ in different seasons or even in different sampling location (not discussed here), the thresholds of RH and $O_3$ for fast sulfate formation further found in our study has its implications on sulfate formation mechanism (see below).

The SORs was further plot against Fe and $NO_2$. No clear dependence of the SOR on concentrations of Fe or $NO_2$ was found (Figs. 8a and 8b). Possible reasons and implications of this result will be discussed in the following section.

### 3.3 Implications for sulfate formation mechanisms

Our observations of the factors that influence sulfate formation have implications for sulfate formation routes and its variations among seasons and pollution conditions.

In retrospect, thresholds in RH and $O_3$ concentrations were found to be critical to the SOR, suggesting that AWC and liquid phase oxidant were two prerequisites for fast multiphase $SO_2$-to-sulfate conversion. $H_2O_2$ and $O_3$ are the two liquid phase oxidants which are responsible for sulfate formation. The $O_3$ oxidation route was proposed not important in high aerosol acidity areas, such as Beijing (Guo et al., 2017; Sievering et al., 2004). A recent study on aerosol pH in Beijing showed that the $PM_{2.5}$ was acidic (RH > 30 %) (Ding et al., 2019), confirming a minor contribution from $O_3$ oxidation. $H_2O_2$ was then the only possible oxidant responsible for sulfate formation. Although direct measurements of aqueous $H_2O_2$ were not performed in this study, the $H_2O_2$ concentrations in Beijing reported by Fu (2014) were found to be positively correlated with temperature. By assuming the reported $H_2O_2$-Temperature relationship applicable to our measurements, a proxy $H_2O_2$ concentration was then estimated. As shown in Fig. S6, maximum concentration of $H_2O_2$ in summer is expected and confirmed, which is in line with the fastest sulfate formation in summer all over the measurement year. SOR was further plotted against $H_2O_2$ and positive correlation was found between them (Fig. S7). In addition, coincident increases in the concentration of $H_2O_2$ and $PM_{2.5}$ in winter of Beijing also lead to an important role of the $H_2O_2$ oxidation route in sulfate formation (Ye et al., 2018). Based on the above discussions, we propose that $H_2O_2$ might be the major oxidant for sulfate formation in Beijing.

The plot of SORs against Fe, the dominant transition metal species, shows no clear dependence (Figs. 8a and S8). Similarly, the plot of SORs against $NO_2$ shows no clear dependence either (Fig. 8b). If Fe acted as a catalyst and thus its concentration might not be directly proportional to SORs. Therefore, such a pattern does not safely exclude TMIs + $O_2$ as a major route for sulfate formation. Several laboratory studies excluded $NO_2$ as a direct oxidant in $SO_2$-to-sulfate conversion. For example, Zhao et al. (2018) tested the oxidation of $SO_2$ by $NO_2$ in an $N_2$ atmosphere and concluded that $NO_2$ is not an important oxidant, since $NO_2$ was more likely to undergo disproportionation (Li et al., 2018). However, Yu et al. (2018) further explored this reaction, and found that the reaction rate was 2–3 orders of magnitude greater in an $O_2$ + $N_2$ atmosphere, indicating potentially important roles of $NO_2$ + $O_2$ oxidation in sulfate formation (He et al., 2014; Ma et al., 2018). As with Fe, if $NO_2$ acted as a catalyst, its concentration might not be directly proportional to that of sulfate. Therefore, such a pattern does

not safely exclude $NO_2 + O_2$ as a major route for sulfate formation either. Although direct aerosol pH measurement is not available here, previous studies has reported a mean aerosol pH value of 4.2 with a low limit of 3.0 in Beijing (Ding et al., 2019; Liu et al., 2017), which suggests that several routes of sulfate formation, including $NO_2 + O_2$, TMIs + $O_2$, $O_3$ oxidation etc., are suppressed. Hence, we carefully propose here neither TMIs +$O_2$ nor $NO_2 + O_2$ seem to be a major route for sulfate formation.

On one hand, a direct measurement of aerosol pH is also urgently needed in the future to examine our proposal here; on another hand, our proposal here has further implication on the understanding of sulfate formation. Previously, aerosol surface area and concentrations of Fe, Mn, and $NO_2$ were used in model evaluations of catalytic sulfate formation in the boundary layer (Wang et al., 2014a; Zheng et al., 2015a). However, our proposals here suggest that a careful reassessment of such calculations is required. In addition, model calculations have often suggested important contributions of in-cloud processes to sulfate accumulation near the ground (Barth et al., 2000), although few observational constraints are available for confirmation of these model results (Harris et al., 2014; Shen et al., 2012). The $O_3$ concentration and RH prerequisites found in the present work might indicate a major role of *in situ* sulfate formation in the boundary layer, via multiphase reactions with $H_2O_2$ as the main oxidant, rather than in-cloud processes and intrusion from the free troposphere.

As the two prerequisites showed strong seasonal and pollution level variations over the measurement year, the SOR exhibited corresponding variations. As shown in Fig. 9, SORs displayed clear seasonal variations, with the highest value (±1 SD) of 0.46 (±0.22) in summer, followed by spring (0.23 ±0.14), autumn (0.18 ±0.15), and winter (0.09 ±0.05). The highest SOR (i.e., fastest $SO_2$-to-sulfate conversion rate) was found in summer, which is not surprising because the ambient conditions in summer were conducive $SO_2$-to-sulfate conversion (Wang et al., 2005). RH and $O_3$ concentrations in summer were not only the highest in the year, but on average were also both higher than their thresholds of 45 % and 35 ppb, respectively, which was unique among the four seasons. In summer, the median and mean (± 1 SD) RH levels were 57.4 % and 57.6 (± 13.6) %, respectively, and the median and mean $O_3$ concentrations were 46.9 ppb and 46.0 (± 18.3) ppb. It should be noted that the median and mean $SO_2$ concentrations were 2.6 and 4.0 (± 3.7) ppb, respectively, which were the lowest in the year. Despite the low concentrations of $SO_2$, there were considerable sulfate concentrations (Figs. 2 and 9), which can be accounted for by fast $SO_2$-to-sulfate conversion. Although the rapid accumulation of secondary sulfate during winter haze days in Beijing has been widely reported (Wang et al., 2014b; Zheng et al., 2015b), the lowest SOR was observed during winter in the present study (Fig. 9a), which is consistent with previous observations (Wang et al., 2005). On winter haze days, RH values of up to 73.6 % and $PM_{2.5}$ mass loadings of up to 375.3 μg $m^{-3}$ were observed. Therefore, AWC was not the limiting factor in $SO_2$-to-sulfate conversion (Figs. 9b and 9e). The $SO_2$-to-sulfate conversion rate in winter could have been limited by the reduced concentration of oxidants (Fig. 9c) as a result of both high emissions of the primary pollutant NO (Fig. S9) and low solar radiation levels (Fig. 9f). Sulfate concentrations in winter were comparable to those in summer, which might have been driven by high $SO_2$ concentrations in winter (Fig. 9d), despite slow $SO_2$-to-sulfate conversion. The lower boundary layer height in winter relative to other seasons would also have encouraged the accumulation of both $PM_{2.5}$ and its components, including

sulfate (Gao et al., 2015; Zhang et al., 2015). The SORs in spring and autumn were comparable and moderate, possibly representing a transition in conditions between summer and winter.

For each season, four pollution scenarios were classified according to $PM_{2.5}$ level. The lowest 25 %, 25–50 %, 50–75 %, and highest 25 % of pollution levels were defined as "clean", "moderate pollution", "heavy pollution", and "severe pollution", respectively. The relative contributions of the seven major known components of $PM_{2.5}$ among the four pollution scenarios are shown in Fig. 10. In all four seasons, the relative contribution of SNA increased with $PM_{2.5}$ loading. This phenomenon has been reported in previous studies, but data availability was limited in autumn (Xu et al., 2017) and winter (Zheng et al., 2015b). The SOR increased consistently in all four seasons as pollution accumulated, where both the highest value and strongest variability were observed in summer (Fig. 11a). Although $SO_2$ should have reduced the SOR (Eq. 1), concurrent increases in primary $SO_2$ and SORs were observed (Figs. 11a and 11b), indicating a significant increase in the $SO_2$-to-sulfate conversion rate with $PM_{2.5}$ loading, which offset the "dilution" effect (Eq. 1). Such variations in sulfate formation with pollution levels can be accounted for by the corresponding variations in both $O_3$ concentrations and RH (Figs. 11c and 11d). In all four seasons, RH increased consistently as pollution accumulated (Fig. 11d). $O_3$ concentrations decreased consistently as pollution evolved in all of the seasons except for summer (Fig. 11c). The distinct variations in $O_3$ during summer, imply strong photochemistry and high concentrations of OH, which might result in a non-negligible contribution of gas phase reactions to the formation of sulfate. However, gas phase reactions alone could not account for the rate of sulfate formation either in Beijing or globally (Finlayson-Pitts and Pitts, 2000; He et al., 2018), due to the relatively slow reaction of $SO_2$ with OH. For example, the lifetime of $SO_2$ with respect to OH oxidation is about 3–4 days, assuming a 24-h average OH concentration of $1 \times 10^6$ molecules $cm^{-3}$ and a pseudo-secondary-order rate constant of $10^{-12}$ $cm^3$ $molecule^{-1}$ $s^{-1}$ (Brothers et al., 2010). However, the overall oxidation lifetime of $SO_2$ is on the order of hours (Berglen et al., 2004; He et al., 2018). Overall, the increase in $SO_2$-to-sulfate conversion with $PM_{2.5}$ loading can be attributed to the self-catalytic nature of the multiphase formation of sulfate, i.e., both RH and $PM_{2.5}$ increased continuously with the accumulation of $PM_{2.5}$, resulting in a rapid rise in AWC and providing greater reaction volume for further sulfate formation. Therefore, the increases in RH and $PM_{2.5}$ could have compensated for the low concentration of oxidants, resulting in fast sulfate formation as pollution evolved. Particularly in summer, not only did both RH and $O_3$ concentrations increase as pollution evolved, but both RH and $O_3$ concentrations were generally above their respective thresholds at all pollution levels (dashed lines in Figs. 11c and 11d). This explains our observations of both the highest values and strongest dependence on pollution level for SORs in summer.

## 4 Conclusions

In this study, the annual mean concentration of $PM_{2.5}$ in Beijing during 2012–2013 was 84.1 (± 63.1) μg $m^{-3}$, with clear seasonal and pollution level variations in its chemical components, highlighting the contribution of SNA formation to the accumulation of $PM_{2.5}$ in all seasons. RH and $O_3$ concentrations were identified as two prerequisites for fast $SO_2$-to-sulfate conversion. RH above a threshold of ~45 % greatly accelerated the conversion rate. A similar effect was also found for $O_3$ at

a concentration threshold of ~35 ppb. Such dependences have interesting implications. First, they indicate a major role of the $H_2O_2$ route in sulfate formation, which might further indicate a major role of *in situ* sulfate production in the boundary layer, rather than in-cloud processes and intrusion from the free troposphere. Second, the observed dependences were also able to account for the seasonal and pollution level variations in $SO_2$-to-sulfate conversion rates. Both the highest value and strongest variability of SOR were observed in summer, which might be attributed to the highest values of $O_3$ concentrations and RH in summer. $SO_2$-to-sulfate conversion accelerated as pollution accumulated, which was primarily attributed to a shift from gas phase oxidation to the multiphase oxidation route, which is self-catalytic in nature. The increase in RH was able to offset the low concentration of oxidants under heavily polluted conditions, and resulted in increasingly fast $SO_2$-to-sulfate conversion as pollution accumulated. While our simultaneous observations of the SOR and concentrations of Fe and $NO_2$ could not exclude TMIs + $O_2$ and $NO_2$-based reactions, a reassessment of the relationships between sulfate formation, aerosol surface area, and the concentrations of Fe and $NO_2$ is necessary. Future quantitative studies of the relative contributions of different sulfate formation routes should include additional measurements, namely $NH_3$ for the proxy calculation of pH values, and $H_2O_2$ to confirm its contribution under different condition.

## Author contributions

TZ designed the study. YHF, CXY, and TZ prepared the manuscript with input from all co-authors. YHF and JXW collected and weighed the $PM_{2.5}$ filter samples and carried out the analysis of the components of $PM_{2.5}$. FFX carried out the measurement of water soluble Fe. YSW and MH provided the data for gaseous pollutants, temperature, and RH. WLL provided the solar radiation data.

## Competing interests.

The authors declare that they have no conflict of interest.

## Acknowledgements

This work was supported by the National Natural Science Foundation Committee of China (91544000, 41121004, and 91744206). We also thank Dr. Robert Woodward-Massey for his kind help in English writing.

### References

Alexander, B., Park, R. J., Jacob, D. J., Li, Q. B., Yantosca, R. M., Savarino, J., Lee, C. C. W., and Thiemens, M. H.: Sulfate formation in sea-salt aerosols: Constraints from oxygen isotopes, J. Geophys. Res., 110, https://doi.org/10.1029/2004JD005659, 2005.

Barth, M. C., Rasch, P. J., Kiehl, J. T., Benkovitz, C. M., and Schwartz, S. E.: Sulfur chemistry in the National Center for Atmospheric Research Community Climate Model: Description, evaluation, features, and sensitivity to aqueous chemistry, J. Geophys. Res. Atmos., 105, 1387-1415, https://doi.org/10.1029/1999jd900773, 2000.

Berglen, T. F., Berntsen, T. K., Isaksen, I. S. A., and Sundet, J. K.: A global model of the coupled sulfur/oxidant chemistry in the troposphere: The sulfur cycle, J. Geophys. Res. Atmos., 109, https://doi.org/10.1029/2003jd003948, 2004.

Brothers, L. A., Dominguez, G., Abramian, A., Corbin, A., Bluen, B., and Thiemens, M. H.: Optimized low-level liquid scintillation spectroscopy of S-35 for atmospheric and biogeochemical chemistry applications, Proc. Natl. Acad. Sci. U.S.A., 107, 5311-5316, https://doi.org/10.1073/pnas.0901168107, 2010.

Cheng, Y. F., Zheng, G. J., Wei, C., Mu, Q., Zheng, B., Wang, Z. B., Gao, M., Zhang, Q., He, K. B., Carmichael, G., Poschl, U., and Su, H.: Reactive nitrogen chemistry in aerosol water as a source of sulfate during haze events in China, Sci. adv., 2, https://doi.org/10.1126/sciadv.1601530, 2016.

Deguillaume, L., Leriche, M., Desboeufs, K., Mailhot, G., George, C., and Chaumerliac, N.: Transition metals in atmospheric liquid phases: Sources, reactivity, and sensitive parameters, Chem. Rev., 105, 3388-3431, https://doi.org/10.1002/chin.200549218, 2005.

Ding, J., Zhao, P., Su, J., Dong, Q., Du, X., and Zhang, Y.: Aerosol pH and its driving factors in Beijing, Atmos. Chem. Phys., 19, 7939-7954, https://doi.org/10.5194/acp-19-7939-2019, 2019.

Ervens, B.: Modeling the processing of aerosol and trace gases in clouds and fogs, Chem. Rev., 115, https://doi.org/10.1021/cr5005887, 2015.

Finlayson-Pitts, B. J., and Pitts, J. N. Jr.: Chemistry of the upper and lower atmosphere: Theory, experiments, and applications, Academic Press, San Diego, Califoria, 2000.

Fu, A. Y.: Study on peroxide concentration and its influence factors in the urban atmosphere, Master, College of Environmental and Resource Sciences, Zhejiang University, Hangzhou, China, 2014 (in Chinese).

Gao, Y., Zhang, M., Liu, Z., Wang, L., Wang, P., Xia, X., Tao, M., and Zhu, L.: Modeling the feedback between aerosol and meteorological variables in the atmospheric boundary layer during a severe fog-haze event over the North China Plain, Atmos. Chem. Phys., 15, 4279-4295, https://doi.org/10.5194/acp-15-4279-2015, 2015.

Gleason, J. F., Sinha, A., and Howard, C. J.: Kinetics of the gas phase reaction $HOSO_2 + O_2$ - $HO_2 + SO_3$, J. Phys. Chem., 91, 719-724, https://doi.org/10.1021/j100287a045, 1987.

Guo, H., Weber, R. J., and Nenes, A.: High levels of ammonia do not raise fine particle pH sufficiently to yield nitrogen oxide-dominated sulfate production, Sci. Rep., 7, 12109, https://doi.org/10.1038/s41598-017-11704-0, 2017.

Han, L., Cheng, S., Zhuang, G., Ning, H., Wang, H., Wei, W., and Zhao, X.: The changes and long-range transport of $PM_{2.5}$ in Beijing in the past decade, Atmos. Environ., 110, 186-195, https://doi.org/10.1016/j.atmosenv.2015.03.013, 2015.

Harris, E., Sinha, B., van Pinxteren, D., Tilgner, A., Fomba, K. W., Schneider, J., Roth, A., Gnauk, T., Fahlbusch, B., Mertes, S., Lee, T., Collett, J., Foley, S., Borrmann, S., Hoppe, P., and Herrmann, H.: Enhanced role of transition metal ion catalysis during in-cloud oxidation of $SO_2$, Science, 340, 727-730, https://doi.org/10.1126/science.1230911, 2013.

Harris, E., Sinha, B., van Pinxteren, D., Schneider, J., Poulain, L., Collett, J., D'Anna, B., Fahlbusch, B., Foley, S., Fomba, K. W., George, C., Gnauk, T., Henning, S., Lee, T., Mertes, S., Roth, A., Stratmann, F., Borrmann, S., Hoppe, P., and Herrmann,

H.: In-cloud sulfate addition to single particles resolved with sulfur isotope analysis during HCCT-2010, Atmos. Chem. Phys., 14, 4219-4235, https://doi.org/10.5194/acp-14-4219-2014, 2014.

He, H., Wang, Y., Ma, Q., Ma, J., Chu, B., Ji, D., Tang, G., Liu, C., Zhang, H., and Hao, J.: Mineral dust and $NO_x$ promote the conversion of $SO_2$ to sulfate in heavy pollution days, Sci. Rep., 4, https://doi.org/10.1038/srep04172, 2014.

He, P., Alexander, B., Geng, L., Chi, X., Fan, S., Zhan, H., Kang, H., Zheng, G., Cheng, Y., Su, H., Liu, C., and Xie, Z.: Isotopic constraints on heterogeneous sulfate production in Beijing haze, Atmos. Chem. Phys., 18, 5515-5528, https://doi.org/10.5194/acp-18-5515-2018, 2018.

Hu, M., Guo, S., Peng, J.-f., and Wu, Z.-j.: Insight into characteristics and sources of $PM_{2.5}$ in the Beijing-Tianjin-Hebei region, China, Nati. Sci. Rew., 2, 257-258, https://doi.org/10.1093/nsr/nwv003, 2015.

Huang, R. J., Zhang, Y. L., Bozzetti, C., Ho, K. F., Cao, J. J., Han, Y. M., Daellenbach, K. R., Slowik, J. G., Platt, S. M., Canonaco, F., Zotter, P., Wolf, R., Pieber, S. M., Bruns, E. A., Crippa, M., Ciarelli, G., Piazzalunga, A., Schwikowski, M., Abbaszade, G., Schnelle-Kreis, J., Zimmermann, R., An, Z. S., Szidat, S., Baltensperger, U., El Haddad, I., and Prevot, A. S. H.: High secondary aerosol contribution to particulate pollution during haze events in China, Nature, 514, 218-222, https://doi.org/10.1038/nature13774, 2014a.

Lelieveld, J., Gromov, S., Pozzer, A., and Taraborrelli, D.: Global tropospheric hydroxyl distribution, budget and reactivity, Atmos. Chem. Phys., 16, 12477-12493, https://doi.org/10.5194/acp-16-12477-2016, 2016.

Li, L., Hoffmann, M. R., and Colussi, A. J.: The role of nitrogen dioxide in the production of sulfate during Chinese haze-aerosol episodes, Environ. Sci. Technol., 52, https://doi.org/10.1021/acs.est.7b05222, 2018.

Li, Y. R., Ye, C. X., Liu, J., Zhu, Y., Wang, J. X., Tan, Z. Q., Lin, W. L., Zeng, L. M., and Zhu, T.: Observation of regional air pollutant transport between the megacity Beijing and the North China Plain, Atmos. Chem. Phys., 16, 14265-14283, https://doi.org/10.5194/acp-16-14265-2016, 2016.

Liang, P., Zhu, T., Fang, Y., Li, Y., Han, Y., Wu, Y., Hu, M., and Wang, J.: The role of meteorological conditions and pollution control strategies in reducing air pollution in Beijing during APEC 2014 and Victory Parade 2015, Atmos. Chem. Phys., 17, 13921-13940, https://doi.org/10.5194/acp-17-13921-2017, 2017.

Liu, M., Song, Y., Zhou, T., Xu, Z., Yan, C., Zheng, M., Wu, Z., Hu, M., Wu, Y., and Zhu, T.: Fine particle pH during severe haze episodes in northern China, Geophys. Res. Lett., 44, 5213-5221, https://doi.org/10.1002/2017GL073210, 2017a.

Liu, X., Sun, K., Qu, Y., Hu, M., Sun, Y., Zhang, F., and Zhang, Y.: Secondary formation of sulfate and nitrate during a haze episode in megacity Beijing, China, Aerosol Air Qual. Res., 2246 - 2257, https://doi.org/10.4209/aaqr.2014.12.0321, 2015.

Liu, Y. C., Wu, Z. J., Wang, Y., Xiao, Y., Gu, F. T., Zheng, J., Tan, T. Y., Shang, D. J., Wu, Y. S., Zeng, L. M., Hu, M., Bateman, A. P., and Martin, S. T.: Submicrometer particles are in the liquid state during heavy haze episodes in the urban atmosphere of Beijing, China, Environ. Sci. Technol. Lett., 4, 427-432, https://doi.org/10.1021/acs.estlett.7b00352, 2017b.

Lu, X., Chen, N., Wang, Y., Cao, W., Zhu, B., Yao, T., Fung, J. C. H., and Lau, A. K. H.: Radical budget and ozone chemistry during autumn in the atmosphere of an urban aite in central China: $RO_x$ budgets and $O_3$ in central China, J. Geophys. Res. Atmos., 122, 3672-3685, https://doi.org/10.1002/2016JD025676, 2017.

Lv, B., Zhang, B., and Bai, Y.: A systematic analysis of $PM_{2.5}$ in Beijing and its sources from 2000 to 2012, Atmos. Environ., 124, 98-108, https://doi.org/10.1016/j.atmosenv.2015.09.031, 2016.

Ma, J., Chu, B., Liu, J., Liu, Y., Zhang, H., and He, H.: $NO_x$ promotion of $SO_2$ conversion to sulfate: An important mechanism for the occurrence of heavy haze during winter in Beijing, Environ. Pollut., 233, 662, https://doi.org/10.1016/j.envpol.2017.10.103, 2018.

Pan, X. L., Yan, P., Tang, J., Ma, J. Z., Wang, Z. F., Gbaguidi, A., and Sun, Y. L.: Observational study of influence of aerosol hygroscopic growth on scattering coefficient over rural area near Beijing mega-city, Atmos. Chem. Phys., 9, 7519-7530, https://doi.org/10.5194/acp-9-7519-2009, 2009.

Quan, J., Liu, Q., Li, X., Gao, Y., Jia, X., Sheng, J., and Liu, Y.: Effect of heterogeneous aqueous reactions on the secondary formation of inorganic aerosols during haze events, Atmos. Environ., 122, 306-312, https://doi.org/10.1016/j.atmosenv.2015.09.068, 2015.

Quan, J. N., Tie, X. X., Zhang, Q., Liu, Q., Li, X., Gao, Y., and Zhao, D. L.: Characteristics of heavy aerosol pollution during the 2012-2013 winter in Beijing, China, Atmos. Environ., 88, 83-89, https://doi.org/10.1016/j.atmosenv.2014.01.058, 2014.

Russell, L. M., and Ming, Y.: Deliquescence of small particles, J. Chem. Phys., 116, 311, https://doi.org/10.1063/1.1420727, 2002.

Sarwar, G., Simon, H., Fahey, K., Mathur, R., Goliff, W. S., and Stockwell, W. R.: Impact of sulfur dioxide oxidation by Stabilized Criegee Intermediate on sulfate, Atmos. Environ., 85, 204-214, https://doi.org/10.1016/j.atmosenv.2013.12.013, 2014.

Seinfeld, J. H., and Pandis, S. N.: Atmospheric chemistry and physics: From air pollution to climate change, Second ed., John Wiley & Sons, New Jersey, 2006.

Shen, X. H., Lee, T. Y., Guo, J., Wang, X. F., Li, P. H., Xu, P. J., Wang, Y., Ren, Y., Wang, W., Wang, T., Li, Y., Cam, S. A., and Collett, J. L.: Aqueous phase sulfate production in clouds in eastern China, Atmos. Environ., 62, 502-511, https://doi.org/10.1016/j.atmosenv.2012.07.079, 2012.

Sievering, H., Cainey, J., Harvey, M., Mcgregor, J., Nichol, S., and Quinn, P.: Aerosol non-sea-salt sulfate in the remote marine boundary layer under clear-sky and normal cloudiness conditions: Ocean-derived biogenic alkalinity enhances sea-salt sulfate production by ozone oxidation, J. Geophys. Res. Atmos., 109, https://doi.org/10.1029/2003jd004315, 2004.

Sun, Y., Wang, Z., Fu, P., Jiang, Q., Yang, T., Li, J., and Ge, X.: The impact of relative humidity on aerosol composition and evolution processes during wintertime in Beijing, China, Atmos. Environ., 77, 927-934, https://doi.org/10.1016/j.atmosenv.2013.06.019, 2013.

Sun, Y. L., Zhuang, G. S., Tang, A. H., Wang, Y., and An, Z. S.: Chemical characteristics of $PM_{2.5}$ and $PM_{10}$ in haze-fog episodes in Beijing, Environ. Sci. Technol., 40, 3148-3155, https://doi.org/0.1021/es051533g, 2006.

Sun, Y. L., Jiang, Q., Wang, Z. F., Fu, P. Q., Li, J., Yang, T., and Yin, Y.: Investigation of the sources and evolution processes of severe haze pollution in Beijing in January 2013, J. Geophys. Res. Atmos., 119, 4380-4398, https://doi.org/10.1002/2014JD021641, 2014.

Vereecken, L., Harder, H., and Novelli, A.: The reaction of Criegee intermediates with NO, $RO_2$, and $SO_2$, and their fate in the atmosphere, Phys. Chem. Chem. Phys., 14, 14682, https://doi.org/10.1039/c2cp42300f, 2012.

Wang, G. H., Zhang, R. Y., Gomez, M. E., Yang, L. X., Zamora, M. L., Hu, M., Lin, Y., Peng, J. F., Guo, S., Meng, J. J., Li, J. J., Cheng, C. L., Hu, T. F., Ren, Y. Q., Wang, Y. S., Gao, J., Cao, J. J., An, Z. S., Zhou, W. J., Li, G. H., Wang, J. Y., Tian, P. F., Marrero-Ortiz, W., Secrest, J., Du, Z. F., Zheng, J., Shang, D. J., Zeng, L. M., Shao, M., Wang, W. G., Huang, Y., Wang, Y., Zhu, Y. J., Li, Y. X., Hu, J. X., Pan, B., Cai, L., Cheng, Y. T., Ji, Y. M., Zhang, F., Rosenfeld, D., Liss, P. S., Duce, R. A., Kolb, C. E., and Molina, M. J.: Persistent sulfate formation from London Fog to Chinese haze, Proc. Natl. Acad. Sci. U.S.A., 113, 13630-13635, https://doi.org/10.1073/pnas.1616540113, 2016.

Wang, Y., Zhuang, G., Tang, A., Yuan, H., Sun, Y., Chen, S., and Zheng, A.: The ion chemistry and the source of $PM_{2.5}$ aerosol in Beijing, Atmos. Environ., 39, 3771-3784, https://doi.org/10.1016/j.atmosenv.2005.03.013, 2005.

Wang, Y., Zhang, Q., Jiang, J., Zhou, W., Wang, B., He, K., Duan, F., Zhang, Q., Philip, S., and Xie, Y.: Enhanced sulfate formation during China's severe winter haze episode in January 2013 missing from current models, J. Geophys. Res. Atmos., 119, 10,425-410,440, https://doi.org/10.1002/2013JD021426, 2014a.

Wang, Y. S., Yao, L., Wang, L. L., Liu, Z. R., Ji, D. S., Tang, G. Q., Zhang, J. K., Sun, Y., Hu, B., and Xin, J. Y.: Mechanism for the formation of the January 2013 heavy haze pollution episode over central and eastern China, Sci. China Earth Sci., 57, 14-25, https://doi.org/10.1007/s11430-013-4773-4, 2014b.

Warneck, P.: The oxidation of sulfur(IV) by reaction with iron(III): a critical review and data analysis, Phys. Chem. Chem. Phys., 20, 4020-4037, https://doi.org/10.1039/c7cp07584g, 2018.

Xie, Y., Ding, A., Nie, W., Mao, H., Qi, X., Huang, X., Xu, Z., Kerminen, V. M., Petäjä, T., and Chi, X.: Enhanced sulfate formation by nitrogen dioxide: Implications from in-situ observations at the SORPES Station, J. Geophys. Res. Atmos., 120, 12679-12694, https://doi.org/10.1002/2015JD023607, 2015.

Xu, F., Qiu, X., Hu, X., Shang, Y., Pardo, M., Fang, Y., Wang, J., Rudich, Y., and Zhu, T.: Effects on IL-1β signaling activation induced by water and organic extracts of fine particulate matter ($PM_{2.5}$) in vitro, Environ. Pollut., 237, 592-600, https://doi.org/10.1016/j.envpol.2018.02.086, 2018.

Xu, L., Duan, F., He, K., Ma, Y., Zhu, L., Zheng, Y., Huang, T., Kimoto, T., Ma, T., Li, H., Ye, S., Yang, S., Sun, Z., and Xu, B.: Characteristics of the secondary water-soluble ions in a typical autumn haze in Beijing, Environ. Pollut., 227, 296-305, https://doi.org/10.1016/j.envpol.2017.04.076, 2017.

Yang, Y. R., Liu, X. G., Qu, Y., An, J. L., Jiang, R., Zhang, Y. H., Sun, Y. L., Wu, Z. J., Zhang, F., Xu, W. Q., and Ma, Q. X.: Characteristics and formation mechanism of continuous hazes in China: a case study during the autumn of 2014 in the North China Plain, Atmos. Chem. Phys., 15, 8165-8178, https://doi.org/10.5194/acp-15-8165-2015, 2015.

Ye, C., Liu, P., Ma, Z., Xue, C., Zhang, C., Zhang, Y., Liu, J., Liu, C., Sun, X., and Mu, Y.: High $H_2O_2$ concentrations observed during haze periods in wintertime of Beijing: Importance of $H_2O_2$-oxidation in sulfate formation, Environ. Sci. Technol. Lett., https://doi.org/10.1021/acs.estlett.8b00579, 2018.

Yu, T., Zhao, D., Song, X., and Zhu, T.: $NO_2$-initiated multiphase oxidation of $SO_2$ by $O_2$ on $CaCO_3$ particles, Atmos. Chem. Phys., 18, 6679-6689, https://doi.org/10.5194/acp-18-6679-2018, 2018.

Zhang, Q., Quan, J. N., Tie, X. X., Li, X., Liu, Q., Gao, Y., and Zhao, D. L.: Effects of meteorology and secondary particle formation on visibility during heavy haze events in Beijing, China, Sci. Total. Environ., 502, 578-584, https://doi.org/10.1016/j.scitotenv.2014.09.079, 2015.

Zhang, R., Jing, J., Tao, J., Hsu, S. C., Wang, G., Cao, J., Lee, C. S. L., Zhu, L., Chen, Z., Zhao, Y., and Shen, Z.: Chemical characterization and source apportionment of $PM_{2.5}$ in Beijing: Seasonal perspective, Atmos. Chem. Phys., 13, 7053-7074, https://doi.org/10.5194/acp-13-7053-2013, 2013.

Zhang, R., Sun, X. S., Shi, A. J., Huang, Y. H., Yan, J., Nie, T., Yan, X., and Li, X.: Secondary inorganic aerosols formation during haze episodes at an urban site in Beijing, China, Atmos. Environ., 177, 275-282, https://doi.org/10.1016/j.atmosenv.2017.12.031, 2018.

Zhang, X. Y., Gong, S. L., Shen, Z. X., Mei, F. M., Xi, X. X., Liu, L. C., Zhou, Z. J., Wang, D., Wang, Y. Q., and Cheng, Y.: Characterization of soil dust aerosol in China and its transport and distribution during 2001 ACE-Asia: 1. Network observations, J. Geophys. Res., 108, https://doi.org/10.1029/2002jd002632, 2003.

Zhao, D., Song, X., Zhu, T., Zhang, Z., Liu, Y., and Shang, J.: Multiphase oxidation of $SO_2$ by $NO_2$ on $CaCO_3$ particles, Atmos. Chem. Phys., 18, 2481-2493, https://doi.org/10.5194/acp-18-2481-2018, 2018.

Zheng, B., Zhang, Q., Zhang, Y., He, K. B., Wang, K., Zheng, G. J., Duan, F. K., Ma, Y. L., and Kimoto, T.: Heterogeneous chemistry: a mechanism missing in current models to explain secondary inorganic aerosol formation during the January 2013 haze episode in North China, Atmos. Chem. Phys., 15, 2031-2049, https://doi.org/10.5194/acp-15-2031-2015, 2015a.

Zheng, G. J., Duan, F. K., Su, H., Ma, Y. L., Cheng, Y., Zheng, B., Zhang, Q., Huang, T., Kimoto, T., Chang, D., Poschl, U., Cheng, Y. F., and He, K. B.: Exploring the severe winter haze in Beijing: the impact of synoptic weather, regional transport and heterogeneous reactions, Atmos. Chem. Phys., 15, 2969-2983, https://doi.org/10.5194/acp-15-2969-2015, 2015b.

Zheng, M., Salmon, L. G., Schauer, J. J., Zeng, L. M., Kiang, C. S., Zhang, Y. H., and Cass, G. R.: Seasonal trends in $PM_{2.5}$ source contributions in Beijing, China, Atmos. Environ., 39, 3967-3976, https://doi.org/10.1016/j.atmosenv.2005.03.036, 2005.

Zhu, T., Shang, J., and Zhao, D. F.: The roles of heterogeneous chemical processes in the formation of an air pollution complex and gray haze, Sci. China Chem., 54, 145-153, https://doi.org/10.1007/s11426-010-4181-y, 2011.

Zhuang, G. S., Guo, J. H., Yuan, H., and Zhao, C. Y.: The compositions, sources, and size distribution of the dust storm from China in spring of 2000 and its impact on the global environment, Chinese. Sci. Bull., 46, 895-901, https://doi.org/10.1007/BF02900460, 2001.

**Figures and Tables**

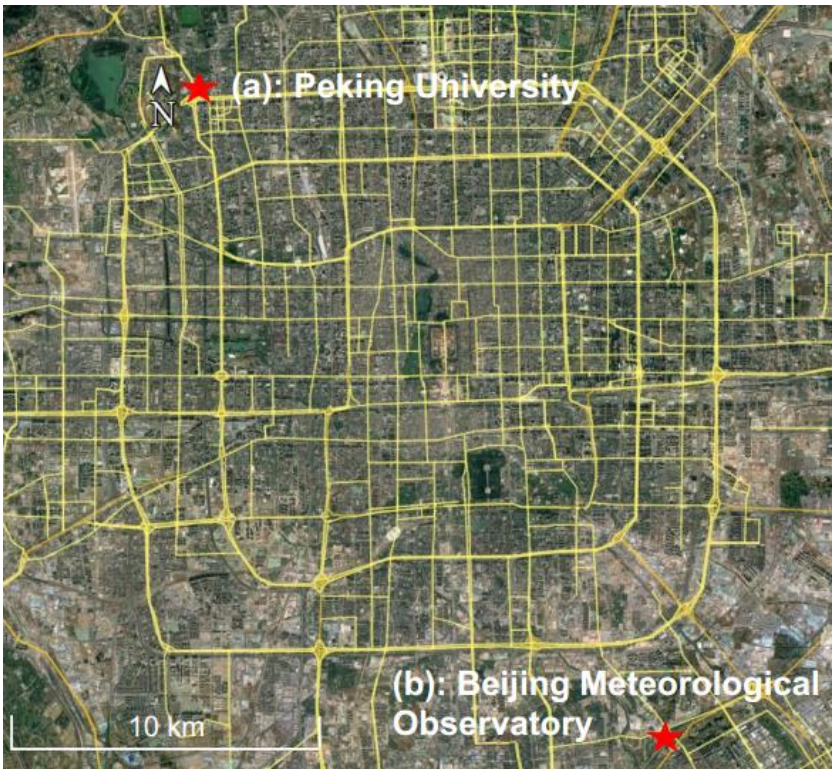


**Figure 1.** Sample sites in this study (red stars): (a) Peking University and (b) Beijing Meteorological Observatory.

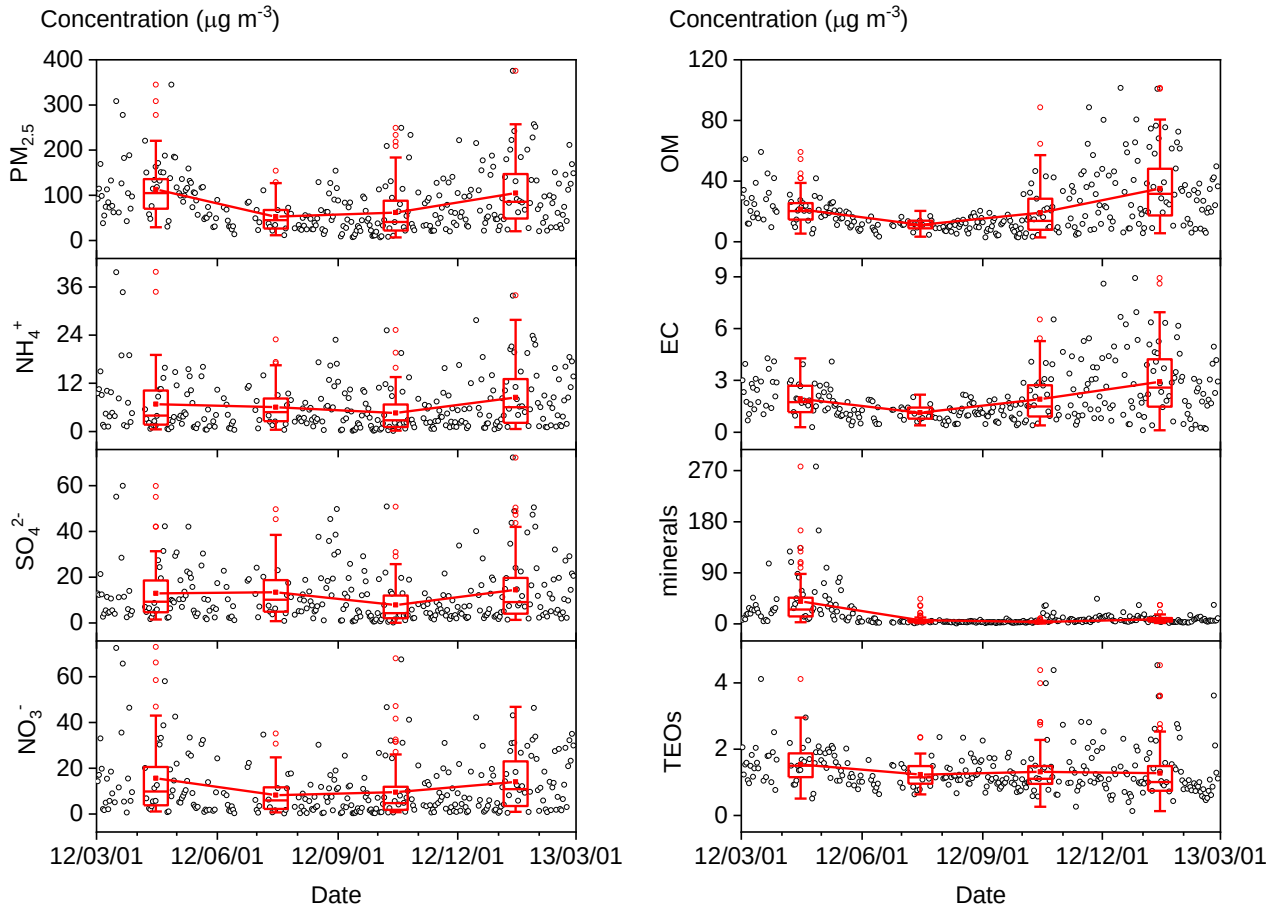


**Figure 2.** Time series of fine particulate matter ($PM_{2.5}$) concentrations and its seven major known components from March 2012 to February 28 2013 (open black circles). The boxes represent, from top to bottom, the 75$^{th}$, 50$^{th}$, and 25$^{th}$ percentiles for each season. The whiskers, solid red squares, and open red circles represent 1.5 times the interquartile range (IQR), seasonal mean values, and outlier data points, respectively.

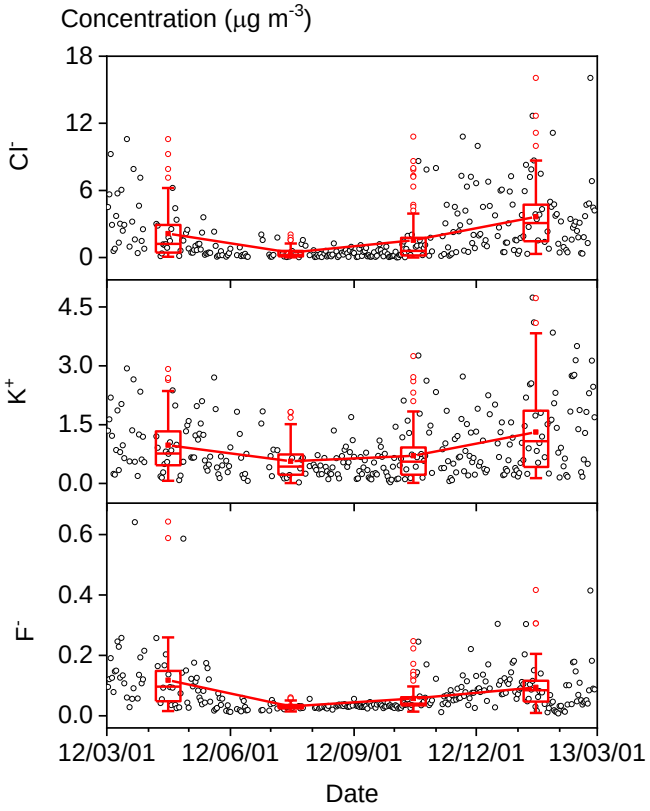


**Figure 3.** Time series of $Cl^-$, $K^+$, and $F^-$ from 1 March 1 2012 to February 28 2013.

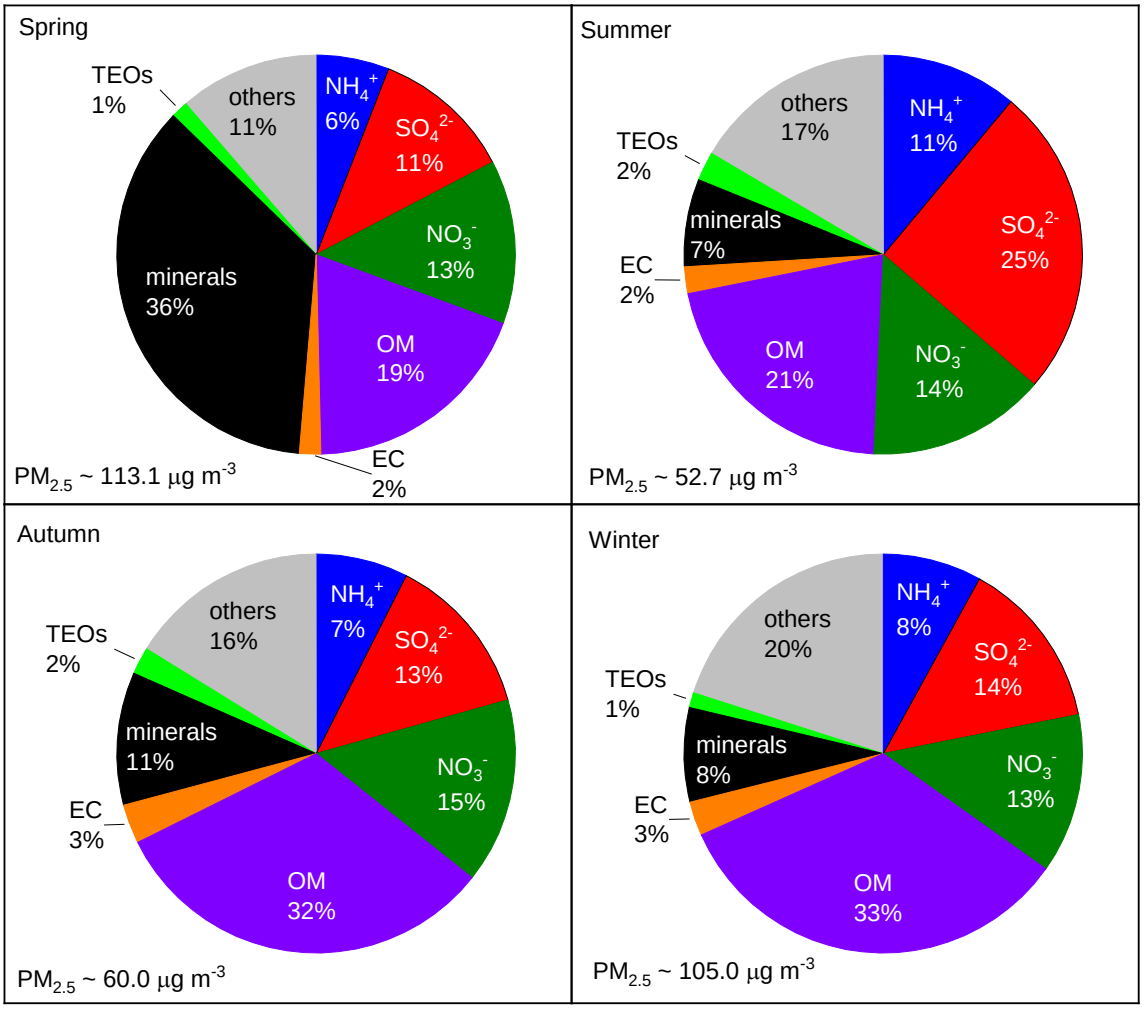


**Figure 4**. Seasonal variations in $PM_{2.5}$ and its eight major components from March 1 2012 to February 28 2013.

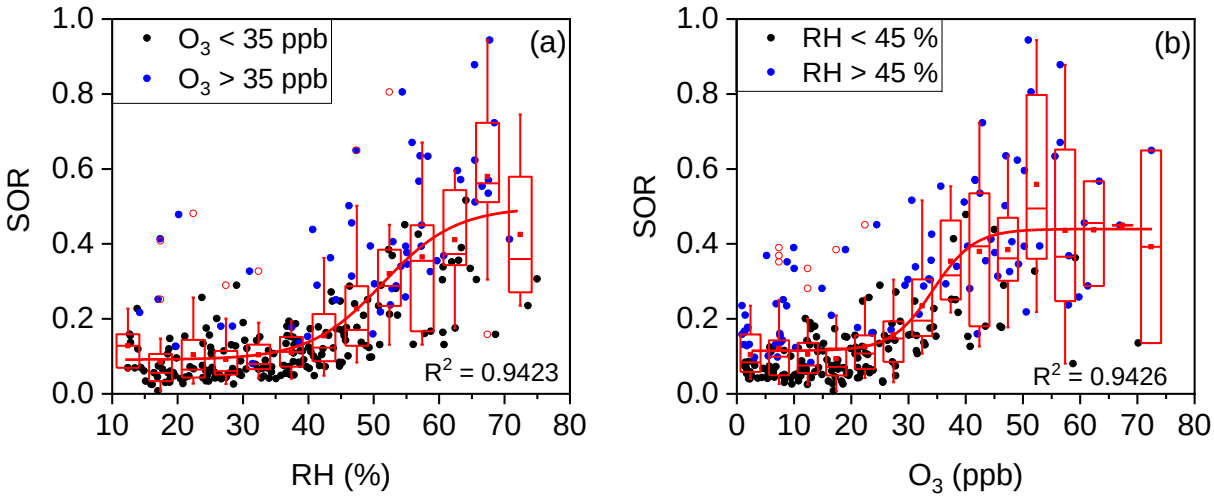


**Figure 5**. (a) Plot of the sulfur oxidation ratio (SOR) against relative humidity (RH) grouped by $O_3$ concentration. The solid blue circles represent $O_3$ > 35 ppb and the solid black circles represent $O_3$ < 35 ppb. (b) Plot of the SOR against $O_3$ grouped by RH. The solid blue circles represent RH > 45 % and the solid black circles represent RH < 45 %. The boxes represent, from top to bottom, the 75$^{th}$, 50$^{th}$, and 25$^{th}$ percentiles in each bin ($\Delta$RH = 5 %; $\Delta O_3$ = 5 ppb). The whiskers, solid red squares, and open red circles represent 1.5 times the IQR, mean values, and outlier data points, respectively. The red lines are best fits to mean values based on a sigmoid function. Data for days with rain or snow were excluded from these plots.

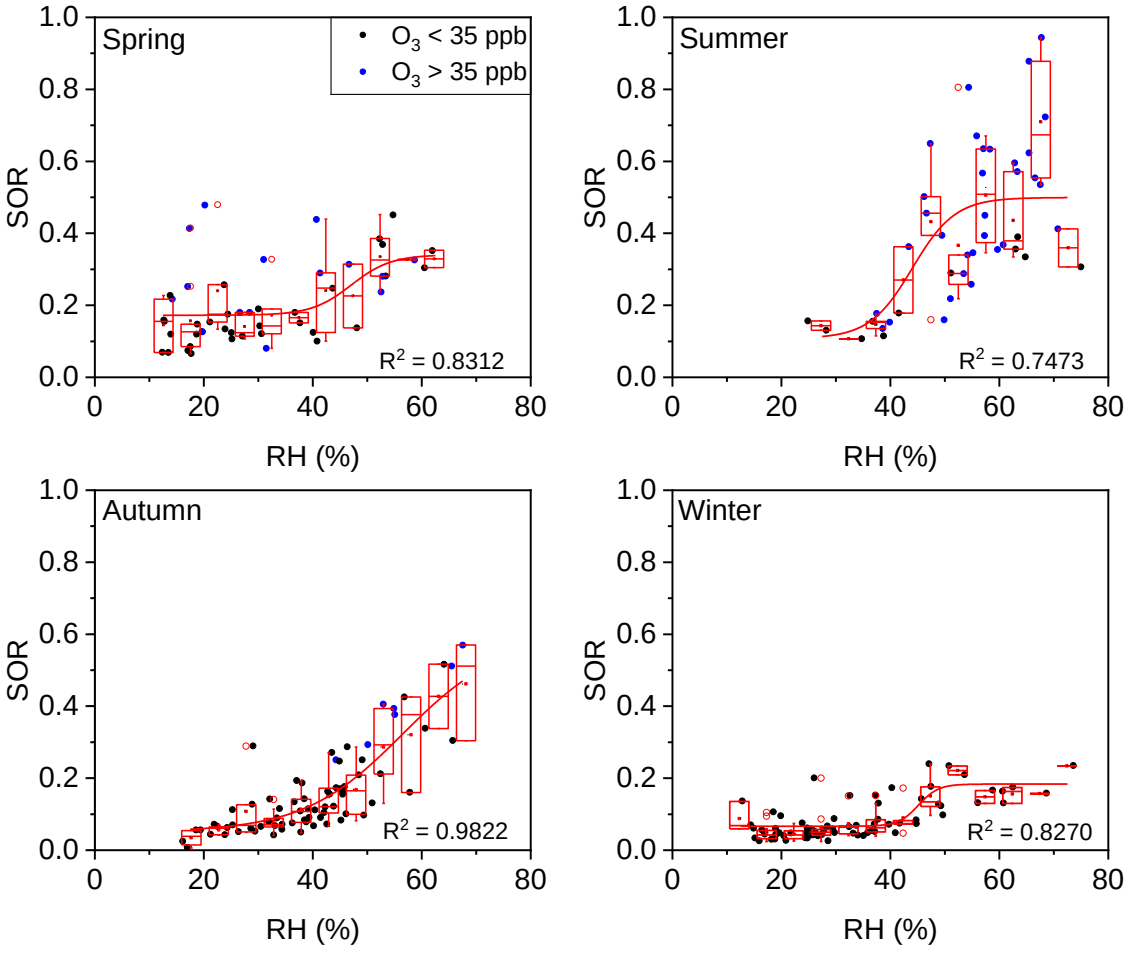


**Figure 6**. Plot of SOR against RH grouped by $O_3$ concentration in four seasons. The solid blue circles represent $O_3$ > 35 ppb and the solid black circles represent $O_3$ < 35 ppb. The boxes represent, from top to bottom, the 75$^{th}$, 50$^{th}$, and 25$^{th}$ percentiles in each bin (ΔRH = 5 %). The whiskers, solid red squares, and open red circles represent 1.5 times the IQR, mean values, and outlier data points, respectively. The red lines are best fits to mean values based on a sigmoid function. Data for days with rain or snow were excluded from these plots.

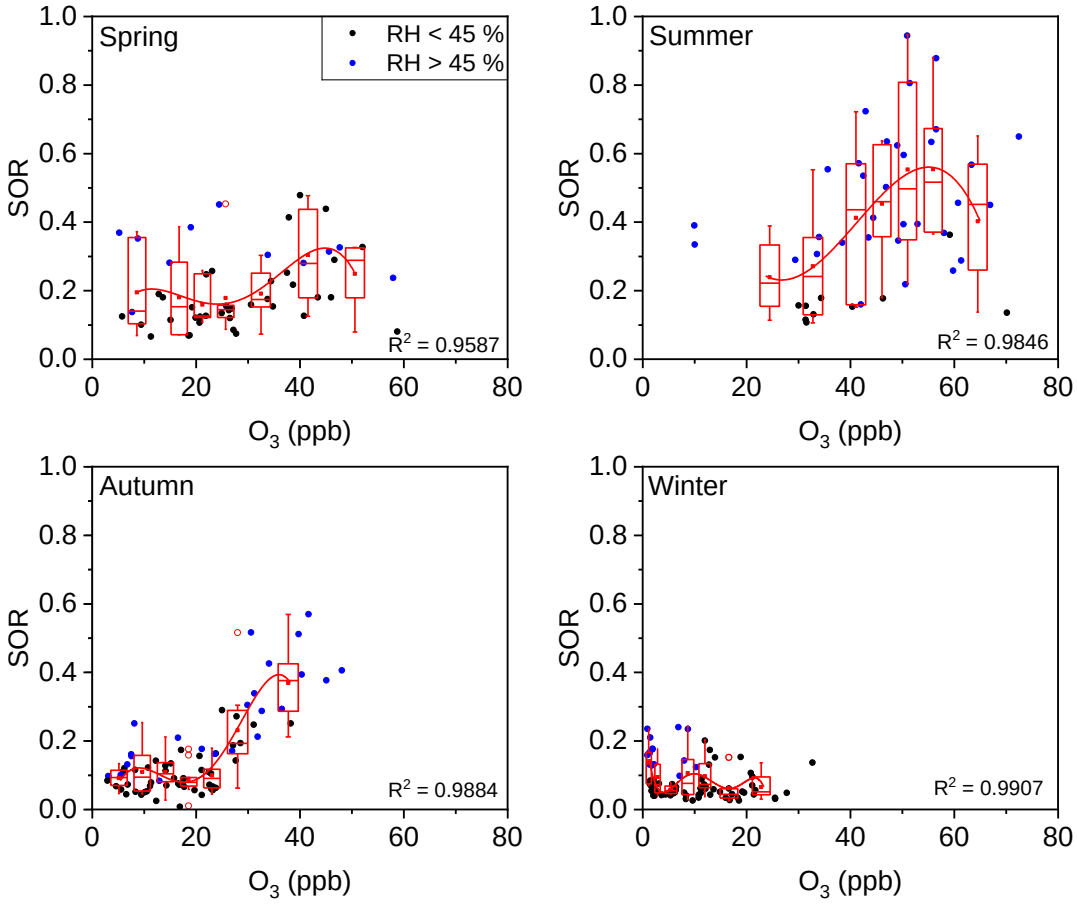


**Figure 7**. Plot of the SOR against $O_3$ grouped by RH. The solid blue circles represent RH > 45 % and the solid black circles represent RH < 45 %. The boxes represent, from top to bottom, the 75$^{th}$, 50$^{th}$, and 25$^{th}$ percentiles in each bin. The bin widths were set such that there were an approximately equal number of data points in each bin The whiskers, solid red squares, and open red circles represent 1.5 times the IQR, mean values, and outlier data points, respectively. The red lines are best fits to mean values based on polynomial functions. Data for days with rain or snow were excluded from these plots.

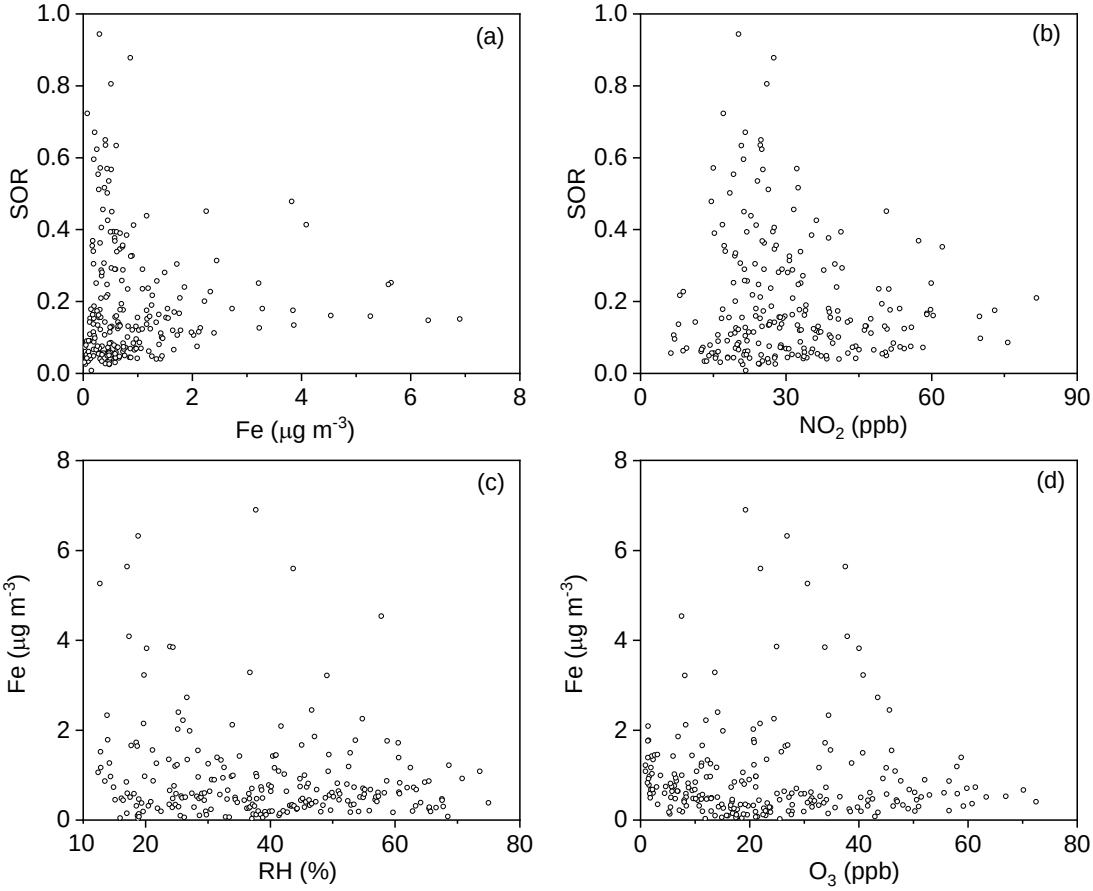


**Figure 8**. Plots of SORs against (a) Fe and (b) $NO_2$. Plots of Fe against (c) RH and (d) $O_3$. Data for days with rain or snow were excluded from these plots.

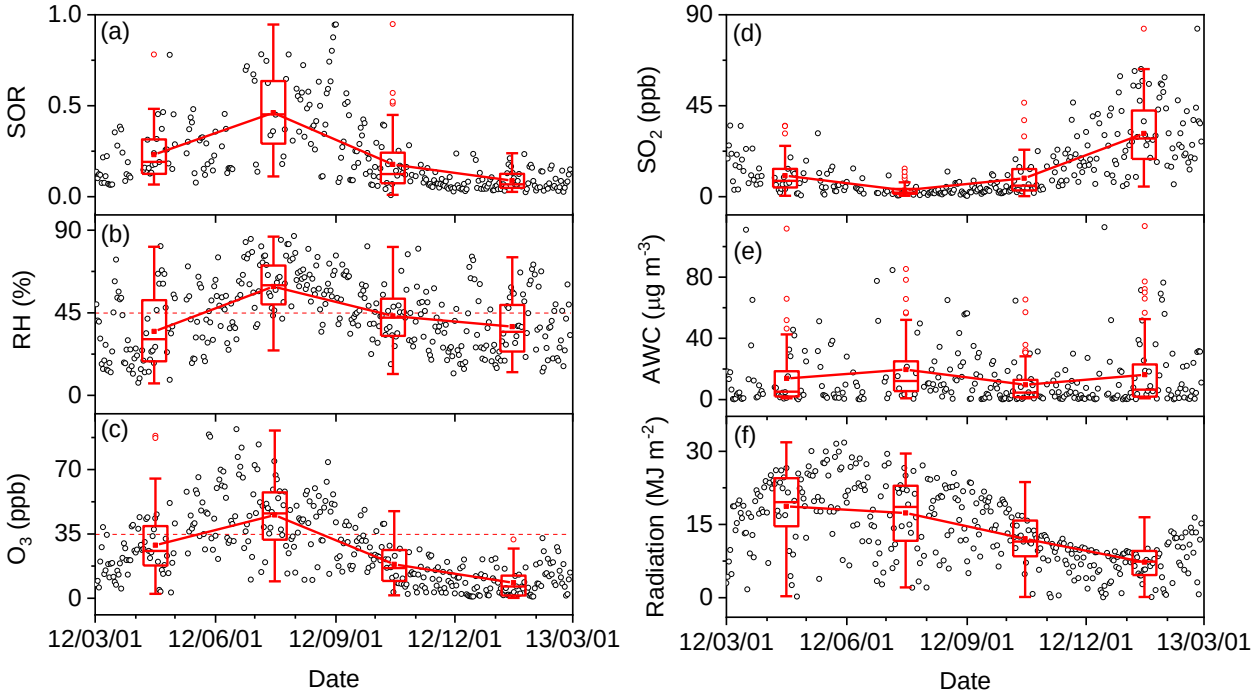


**Figure 9**. Time series of (a) SORs, (b) RH, (c) $O_3$, (d) $SO_2$, (e) aerosol water content (AWC), and (f) solar radiation from March 1 2012 to February 28 2013 (open black circles). The boxes represent, from top to bottom, the 75$^{th}$, 50$^{th}$, and 25$^{th}$ percentiles for each season. The whiskers, solid red squares, and open red circles represent 1.5 times the IQR, seasonal mean values, and outlier data points, respectively. The horizontal dashed lines in panels (b) and (c) represent thresholds of RH = 45 % and $O_3$ = 35 ppb, respectively.

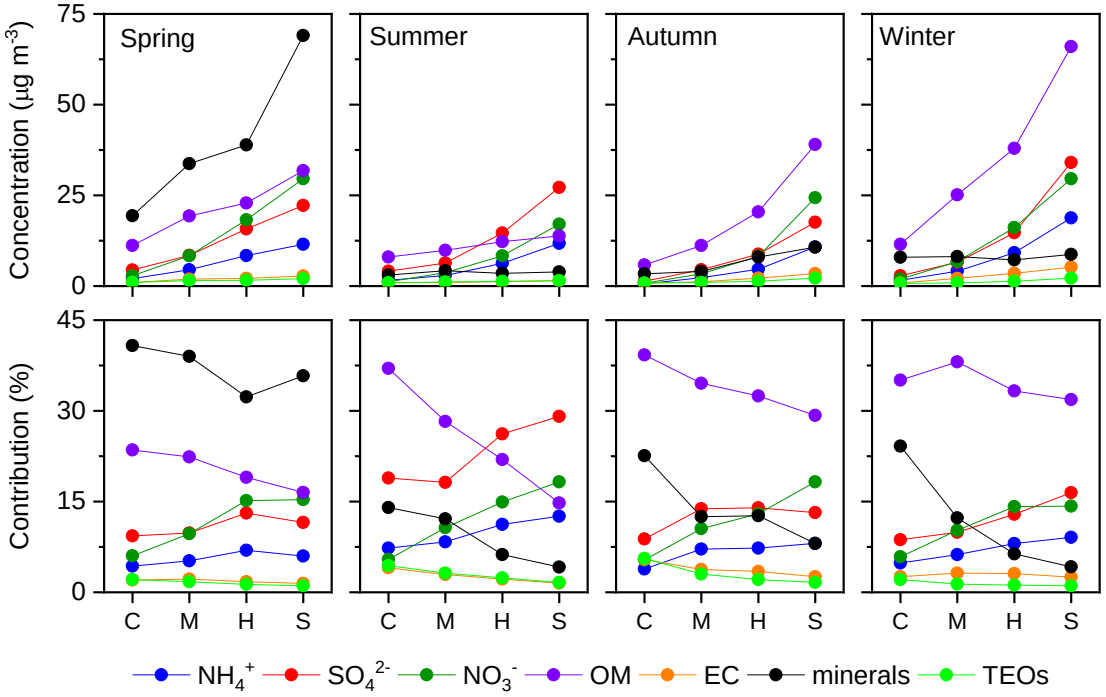


**Figure 10**. Variations in the mean concentrations (upper panels) and contributions (lower panels) of the seven major known components of $PM_{2.5}$ with pollution levels in each season. C, clean; M, moderate pollution; H, heavy pollution; S, severe pollution.

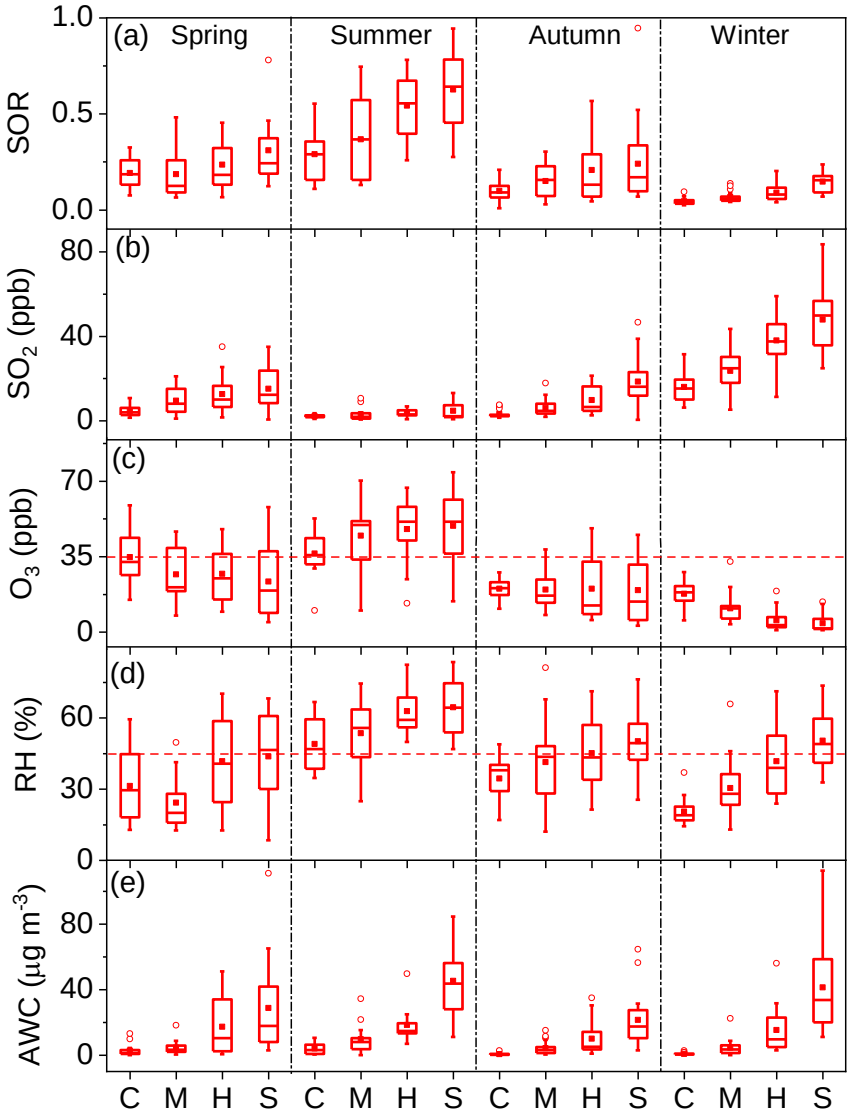


**Figure 11**. Variations in (a) SORs, (b) $SO_2$, (c) $O_3$, (d) RH, and (e) AWC with pollution levels in each season. C, clean; M, moderate pollution; H, heavy pollution; S, severe pollution. The boxes represent, from top to bottom, the 75$^{th}$, 50$^{th}$, and 25$^{th}$ percentiles for each pollution level. The whiskers, solid red squares, and open red circles represent 1.5 times the IQR, mean values, and outlier data points, respectively. The horizontal dashed lines in panels (c) and (d) represent thresholds of $O_3$ = 35 ppb and RH = 45 %, respectively.

**Table 1**. Annual and seasonal mean concentrations (μg $m^{-3}$, ± 1 standard deviation) of $PM_{2.5}$ and its seven major known components.

| Component | Annual | Spring | Summer | Autumn | Winter |
|---|---|---|---|---|---|
| **$PM_{2.5}$** | 84.1 ± 63.1 | 113.1 ± 62.0 | 52.7 ± 32.6 | 60.0 ± 51.3 | 105.0 ± 71.7 |
| **$NH_4^+$** | 6.4 ± 6.4 | 6.7 ± 7.3 | 5.9 ± 5.0 | 4.5 ± 4.8 | 8.4 ± 7.4 |
| **$SO_4^{2-}$** | 12.0 ± 12.2 | 12.9 ± 12.4 | 13.3 ± 11.5 | 7.9 ± 8.7 | 14.5 ± 14.4 |
| **$NO_3^-$** | 11.5 ± 12.6 | 15.0 ± 16.0 | 7.6 ± 8.0 | 9.0 ± 11.8 | 13.6 ± 12.1 |
| **OM** | 22.7 ± 18.1 | 21.5 ± 10.5 | 11.1 ± 3.8 | 19.2 ± 16.1 | 35.2 ± 23.4 |
| **minerals** | 14.7 ± 27.0 | 40.7 ± 45.0 | 3.7 ± 1.6 | 6.5 ± 7.0 | 8.0 ± 5.6 |
| **TEOs** | 1.3 ± 0.7 | 1.5 ± 0.6 | 1.2 ± 0.4 | 1.3 ± 0.7 | 1.3 ± 0.8 |
| **EC** | 2.1 ± 1.5 | 1.9 ± 1.0 | 1.1 ± 0.5 | 1.9 ± 1.3 | 2.9 ± 2.0 |